ELSEVIER

Scopus

doi

# Journal of Vibration Engineering

ISSN:1004-4523

Registered

- SCOPUS
- GOOGLE SCHOLAR
- DIGITAL OBJECT IDENTIFIER (DOI)
- IMPACT FACTOR 6.1

Our Website
www.jove.science

# Statistical Estimation of Point Refractivity Gradient and Geoclimatic Factor at Microwave Antenna Height in Port Elizabeth, South Africa

Y. B. Lawal[1*], O. A. Layioye[2], P. A. Owolawi[3], C. Tu[4], E. Van Wyk[5], and J. S. Ojo[6]
[1,2,3,4]Department of Computer Systems Engineering, Tshwane University of Technology, South Africa
[5]Faculty of Information and Communications Technology, Tshwane University of Technology
[6]Department of Physics, Federal University of Technology, Akure, Nigeria

***Abstract:*** *Geoclimatic factor is a crucial local radio propagation metric that must be considered to achieve efficient wireless link design, particularly during the worst weather condition. This study investigated the seasonal and interannual behaviour of surface refractivity gradients and the geoclimatic factor K for terrestrial microwave link design over Port Elizabeth, South Africa, using ERA5 reanalysis data from 2016–2024. The analysis applied ITU-R P.453-14 and P.530-19 formulations to derive hourly gradients and the corresponding K values based on the 1% exceedance criterion. Results show that the overall annual mean geoclimatic factor is approximately* $9.86 \times 10^{-5}$. *Seasonally, summer exhibits the highest mean value of* $10.22 \times 10^{-5}$ *due to enhanced moisture availability and stronger vertical refractivity stratification. Autumn (*$9.82 \times 10^{-5}$ *and spring (*$9.71 \times 10^{-5}$*) show moderate gradients, reflecting transitional atmospheric stability. Winter records the lowest mean of about* $9.34 \times 10^{-5}$*, consistent with reduced humidity and more stable boundary-layer conditions. The annual trend indicates significant interannual variability, with a notable minimum in 2021 attributable to anomalous synoptic-scale circulation and post-La Niña moisture suppression, which weakened vertical refractivity gradients. These findings highlight the sensitivity of K to regional climatic fluctuations and emphasize the need for location-specific values rather than relying solely on global ITU-R statistics. The results provide refined K estimates for improved path-clearance, ducting-avoidance strategies, and fade-margin planning, offering practical guidance for resilient communication system design under varying atmospheric conditions in Port Elizabeth and its environs.*

***Keywords:*** *Atmospheric Refractivity, Refractivity Gradient, Geoclimatic Factor, Tropospheric Propagation, Surface Ducting, Super-refraction, Terrestrial Microwave Link.*

## 1.0 INTRODUCTION

The atmospheric condition governed by some climatic parameters poses great threats to the planning and quality of inter-terrestrial radio links. Radio-meteorological parameters such as refractivity gradient and geoclimatic factor dominate the bending, focusing and fading of microwave signals in the atmosphere [1]-[2]. These parameters are functions of the refractive index usually expressed as refractivity $N$, and depend on basic atmospheric parameters such as pressure, temperature, and water vapor pressure. The vertical derivative of the refractive index describes the refractivity gradient

*Corresponding Author

$dN/dh$, which is a determining factor of whether propagation is considered as ducting, super-refractive, standard, or sub-refractive [2]-[4]. According to ITU-R P.453-14, even moderate changes in low-level temperature and humidity can adequately alter the profiles of refractivity, and hence the curvature of radio waves in the first kilometer above ground [5]. The geoclimatic factor $K$ is an exponential function of the point refractivity gradient in the lowest tens of meters. The terrestrial line-of-sight (LOS) multipath fade depth estimation is highly feasible by determining the refractivity gradient and geoclimatic factor, as established in ITU-R P.530-19 [6]-[7]. The $dN/dh$ and $K$ phenomena jointly control the effective earth radius, beam spreading, surface and atmospheric multipath, and $k$-type diffraction fading on high-capacity microwave backbones, 5G/6G backhaul, and radar systems [8]-[10]. In environments such as the coastal and subtropical areas, strong surface inversions, sea-breeze fronts, and moisture advection can result in super-refractive layers and ducts that severely reduce the availability of the link, however, can also be exploited for wider-range over the horizon coverage [10]-[11]. For dense terrestrial networks, estimating site-specific statistics of point refractivity gradient and geoclimatic factor at microwave antenna height are important data for modern radio-climatic characterization and link budget design.

The statistical estimation of refractivity gradient and geoclimatic factor depends on indirect measurements of pressure, temperature and humidity from surface stations, radiosondes, satellites, or numerical reanalysis products [2]. Traditional methods of estimating refractivity and its vertical profiles in the lowest 65 to 100 m utilize radiosonde profiles, and $K$ is computed using the point gradient not exceeded for 1% of an average year [12]-[13]. Recent investigations have shown that satellite-derived and reanalysis meteorological data can reliably reproduce refractivity and its gradients over data-sparse regions, especially when validated against radiosondes and ground-based measurements [14]-16]. Statistical analyses from several literatures have consistently reported that relative humidity and temperature are the dominant drivers of seasonal refractivity and field-strength variability, emphasizing their significance in parameterizing refractivity gradient and $K$ for terrestrial links planning [2], [17]-[18].

Extensive work has been done on the characterization of refractivity gradient and geoclimatic factor across diverse climatic regimes. For the tropical climate, several authors have reported strong seasonal modulation of $dN/dh$ and $K$ using radiosonde, satellite, and surface meteorological data, with super-refraction and ducting frequently observed in coastal stations. Etokebe [13] derived monthly and seasonal $dN_1$ and $K$ for Calabar, a costal location in Nigeria, showing higher geoclimatic factors in the dry season and lower values during the rainy months. Emmanuel [17] and Oluwafemi and Olla [19] extended this framework to multiple Nigerian stations, providing national-scale $K$ maps for radio-link design. In Yenagoa, Lawal and Omotoso [2] applied ECMWF reanalysis to compute point refractivity gradient and geoclimatic factor at 70 m, revealing predominantly super-refractive and ducting conditions and highlighting the sensitivity of $K$ to local coastal climate. Several studies have also been carried out across other climatic regimes by other researchers. Bettouche et al [12] evaluated $dN_1$ and $K$ at 65 m in Quebec, while Arctic and mid-latitude studies have demonstrated that low-level inversions and strong humidity gradients produce large temporal variability in geoclimatic factor. In Southern Africa, Nyete and Afullo [10], Odedina and Afullo [11], Palmer and Baker [20] and other subsequent works have interpolated k-factor and $K$ fields from radiosonde-derived refractivity gradients and linked them to diffraction fading and multipath statistics on terrestrial microwave links. These regional studies, together with recent contributions by Palmer and Baker [21] on long-term average of the effective earth radius factor and Lawal et al [16] and [22] on rain heights

*Corresponding Author

climatology and rain-induced attenuation over South Africa, emphasize the need for refined local radio-climate parameters to support high-capacity links.

Despite all the progresses made on the determination of radio refractivity and geoclimatic factor across the sub-tropics, very limited work has focused specifically on the statistical estimation and cumulative distribution of point refractivity gradient and geoclimatic factor at microwave-antenna height in Port Elizabeth (Gqeberha), a maritime city situated along Algoa Bay on the south-eastern coast of South Africa. The region is characterized by a relatively mild but windy coastal climate, persistent marine boundary-layer inversions, frequent fog episodes, and intermittent wind-driven coastal upwelling that modulate near-surface temperature and humidity fields [23]. These features are likely to produce distinct refractivity-gradient and $K$ statistics compared with previously studied inland or other coastal locations in South Africa. Building on earlier refractivity and k-factor mapping studies in Southern Africa [11], the present work uses high-resolution ERA5 hourly temperature, pressure, and humidity data at three pressure levels (surface, 1000 hPa, and 975 hPa) to interpolate refractivity, point refractivity gradient, and geoclimatic factor at 65 m over Port Elizabeth. The resulting local statistics are expected to provide more realistic $K$ values for link-budget design, strengthen radio-climate characterization for the Eastern Cape, and ultimately improve the reliability of terrestrial microwave links and emerging high-throughput services operating over this climatically sensitive coastal corridor.

## 2.0 THEORETICAL AND MATHEMATICAL BACKGROUND

### 2.1 Determination of Refractivity, Refractivity Gradient, and Geoclimatic Factor

The variation in pressure, temperature and water vapor content causes changes in the refractive index of moist air, $n$, resulting in tropospheric refraction. It is appropriate to define the radio-refractivity $N$ in "*N-unit*" by [11]:

$$n = 1 + N \times 10^{-6}, \tag{1}$$

The widely used expression for $N$ (for frequencies below about 100 GHz) as a function of atmospheric pressure $P$ (hPa), absolute temperature $T$ (K) and water-vapor pressure $e$ (hPa) is given by the ITU-R P.453-14 as [5];

$$N = 77.6\,\frac{P}{T} + 3.73 \times 10^{5}\,\frac{e}{T^{2}}. \tag{2}$$

The water vapor pressure $e$ is determined from relative humidity $H$ (%) using a saturation vapor pressure $e_s$ relation given by:

$$e = H \times \frac{e_s(t)}{100}, \tag{3}$$

$$e_s(t) = 6.1121 \exp\left[\frac{17.502\,t}{t+240.97}\right], \tag{4}$$

where $t$ is the air temperature in °C.

The bending of the radio rays is determined by the vertical structure of $N$. The refractivity gradient $dN/dh$ over a small height interval $\Delta h$ can be approximated by the finite-difference form given by [2]:

$$\frac{dN}{dh} \approx \frac{N_2 - N_1}{h_2 - h_1}, \tag{5}$$

*Corresponding Author

where $N_1$ and $N_2$ are refractivities at heights $h_1$ and $h_2$.

The $K$ established in ITU-R P.530-19 parameterizes the local tendency for multipath fading and is linked empirically to the worst-month statistics of the point refractivity gradient in the lowest tens of meters (ITU-R, 2025) [6]. The ITU regression model, as adopted in recent tropical and subtropical studies, is given as [2], [6] & [11]:

$$K = 10^{-4.6-0.0027\,dN_1}, \tag{6}$$

where $dN_1$ (*N-unit* $km^{-1}$) is the point refractivity gradient in the lowest 65 m not exceeded for 1 % of an average year.

### 2.2 Relationship between Refractivity Gradient and Atmospheric Refraction Regimes

The mathematical quantities defined above $N$, $dN/dh$ and $K$ provide a compact description of the physical refraction regimes schematically illustrated in Figure 1, where four representative ray trajectories are labelled as sub-refraction, standard refraction, super-refraction and ducting. In a standard atmosphere, the refractivity gradient in the lowest hundred meters is close to $-40$ *N-unit* $km^{-1}$, the corresponding effective earth radius factor, $k \approx 4/3$ yields rays that gently curve towards the Earth which therefore causes the extension of the radio horizon beyond the geometric line of sight [9] & [24]. This case is illustrated in the figure 1 by the dashed ray labelled "standard refraction," which lies between the sub-refracted and super-refracted paths.

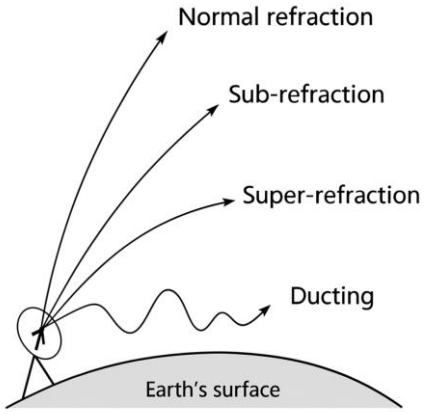


Figure 1. Common classification of atmospheric refraction conditions

Deviations of $dN/dh$ from this standard value produce abnormal refraction conditions. Following Hall's classification and subsequent radio-climatological studies, a commonly adopted set of thresholds is given as [25] & [26}:

Sub-refraction: $\frac{dN}{dh} > -40\ N\ km^{-1}$, (7)

Standard refraction: $\frac{dN}{dh} = -40\ N\ km^{-1}$, (8)

Super-refraction: $-157 < \frac{dN}{dh} < -40\ N\ km^{-1}$, (9)

Ducting (trapping): $\frac{dN}{dh} < -157\ N\ km^{-1}$, (10)

*Corresponding Author

In sub-refraction, the rays bend less than the curvature of the earth, resulting in reduction in coverage and increased diffraction loss. For super-refraction, there is a stronger downward bending. Whereas, for ducting, this represents an extreme case of refraction where there is a rapid reduction in refractivity with height, that the ray curve exceeds that of the Earth [15], [25], [27]-[28]. The higher likelihood of deep multipath fading which is a function of larger $K$ values is as a result of stronger super-refraction or ducting, which corresponds to more negative gradients [6].

## 3.0 METHODOLOGY

### 3.1 Research Location and Data Acquisition

This study focuses on Port Elizabeth (Gqeberha), a coastal city located along Algoa Bay in the Eastern Cape Province of South Africa, with coordinates 33.96°S, 25.60°E. The region is characterized by a temperate maritime climate with persistent sea breezes, frequent low-level inversions and sharp humidity gradients, all of which strongly influence near-surface refractivity and ducting occurrence. Port Elizabeth, like the rest of South Africa, experiences four distinct seasons each year. Winter occurs from June to August (JJA), spring spans September to November (SON), summer extends from December to February (DJF), and autumn runs from March to May (MAM) [23]. The atmospheric data set used in this work is the ERA5 reanalysis found in the database of Copernicus Climate Change Service (C3S), produced by the European Centre for Medium-Range Weather Forecasts (ECMWF), which provides hourly data of pressure, temperature, and humidity on a 0.25° grid from 1979 to the present [29]. For this work, the grid cell whose center is closest to Port Elizabeth was extracted and eight years hourly data between 2016 and 2023 at the surface, 1000 hPa and 975 hPa pressure levels were retained. Dew-point temperature and relative humidity from ERA5 were used to derive water vapor pressure for refractivity computation following the recommendation in ITU-R P.453-14 [5]. The study period 2016 to 2023 was chosen to provide a multi-year climatology suitable for robust estimation of diurnal, monthly and seasonal statistics of refractivity gradient and geoclimatic factor.

### 3.2 Computation of Refractivity Gradient and Geoclimatic Factor

For each ERA5 pressure level, radio refractivity $N$ was computed from hourly pressure $P$ (hPa), air temperature $T$ (K) and water vapor pressure $e$ (hPa) using the standard Smith–Weintraub-type expression given by equation (2), recommended in ITU-R P.453-14 [5]. Refractivity at 65 m (nominal microwave antenna height) was obtained by vertical interpolation between the surface, 1000 hPa and 975 hPa levels, assuming a monotonic variation of $P$ with height and using hydrostatic and hypsometric relationships as provided in previous refractivity-gradient studies (Adediji et al., 2011) [9]. The point refractivity gradient $dN_1$ in the lowest 65 m was then approximated by a finite-difference [5]:

$$dN_1 \approx \frac{N_{65}-N_0}{0.065}\,[N\text{-}unit\ km^{-1}] \tag{11}$$

where $N_0$ and $N_{65}$ denote refractivity at the surface and 65 m, respectively.
For each hour, the corresponding geoclimatic factor $K$ was evaluated from the ITU-R P.530-19 regression model, given by equation (6), which links the 1-percentile point refractivity gradient in the lowest 65 m to the severity of multipath fading on terrestrial links. Hourly values of $dN_1$ and $K$ were then aggregated to construct diurnal cumulative distribution functions (CDFs), monthly and seasonal statistics, and annual trends. The 1% not exceeded (i.e., 99th-percentile) values of $dN_1$ and $K$ for an average day and an average year were

*Corresponding Author

extracted from the empirical CDFs, in accordance with ITU-R definitions and with earlier works over Nigeria and Southern Africa.
In the present study, refractivity at microwave antenna height (65 m) is obtained by vertical interpolation from ERA5 fields at the three pressure levels, and the point refractivity gradient $dN_1$ in the lowest 65 m is computed using the refractivity difference between the surface and 65 m. This approach follows previous work using radiosonde data to estimate near-surface gradients for link design [11].

## 4.0 RESULTS AND DISCUSSION

This section presents results and discusses the refractivity gradient and geoclimatic-factor ($K$) behaviour at a typical terrestrial antenna height of 65 m above ground level (AGL) over Port Elizabeth, South Africa, using hourly ERA5 meteorology mapped to height via pressure-level information and the hypsometric relation. Surface refractivity $N$ was computed from pressure, temperature and humidity using the ITU-R P.453-14 formulation in equation (2) and point refractivity gradients $dN/dz$ were derived by local finite differencing about the 65 m level followed by corresponding the geoclimatic factor using ITU-R P.530-19 procedure. The diurnal structure by season was examined using both cumulative probability distribution curves (CPDCs) and 1% diurnal envelopes and presented in sub-section 4.1. The behaviour of refractivity gradient and geoclimatic-factor were condensed into monthly and seasonal statistics and reported in sub-section 4.2. The interannual trend of $K$ was reported in sub-section 4.3, drawing out practical implications for terrestrial link engineering on the south coast as presented in sub-section 4.4.

### 4.1 Diurnal Variation of Refractivity Gradient during the seasons

Figures 2–3 depict the seasonal diurnal behaviour of the point refractivity gradient at 65 m. Figure 2 shows season-stratified CPDCs of hourly refractivity gradient. The steeper left-tails indicate a higher frequency of strongly negative gradients, i.e., enhanced super-refraction/ducting propensity. It could be observed that at lower percentage of exceedance, the winter season is highly prone to anomalous propagations, followed by autumn, while the summer is less susceptible. Highly negative value is influenced by temperature inversion, a highly predominant phenomenon in the morning hours during the winter and autumn in southern Africa as depicted in Figure 3 [30]. This is consistence with similar research in Indian which reported high occurrence super-refraction and ducting in the winter [31]. Figure 3 is the season diurnal lines of the 1% not-to-be-exceeded gradient (within an average day) which reveals the timing of most adverse conditions. As expected for a coastal site influenced by land–sea-breeze circulations and nocturnal boundary-layer stabilization, night-time to early-morning hours tend to exhibit more negative gradients than the mid-afternoon when convective mixing erodes vertical moisture and temperature stratification. This canonical pattern, i.e. stable nights with more negative dN/dz; convective afternoons with less negative dN/dz, is evident in the hourly 1% envelopes presented in Figure 3. The figure reveals that refractivity gradient generally dips before sunrise and rises during local noon. The CPDCs in Figure 2 further show that seasonal separation is modest compared with the diurnal signal, but still discernible: the season(s) with more frequent strong inversions (e.g., driven by colder marine air, frontal passages, or persistent nocturnal stability) display heavier left-tails, while seasons with more vigorous daytime mixing yield lighter tails.

*Corresponding Author

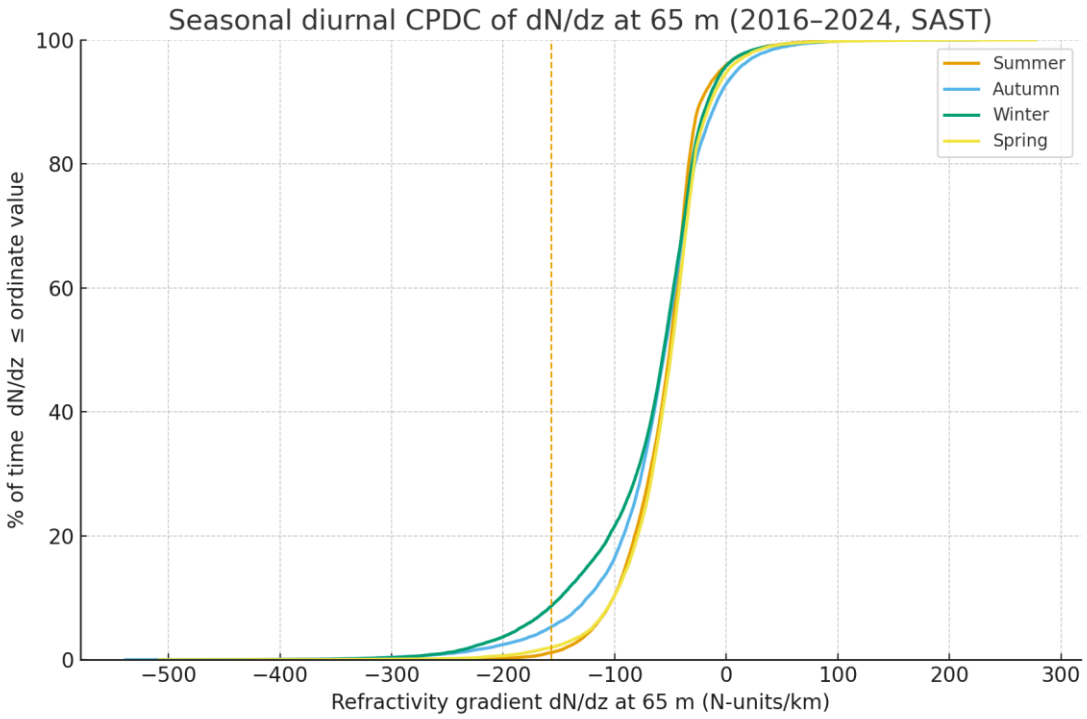


Figure 2. Cumulative Probability Distribution Curve of Diurnal Refractivity Gradient

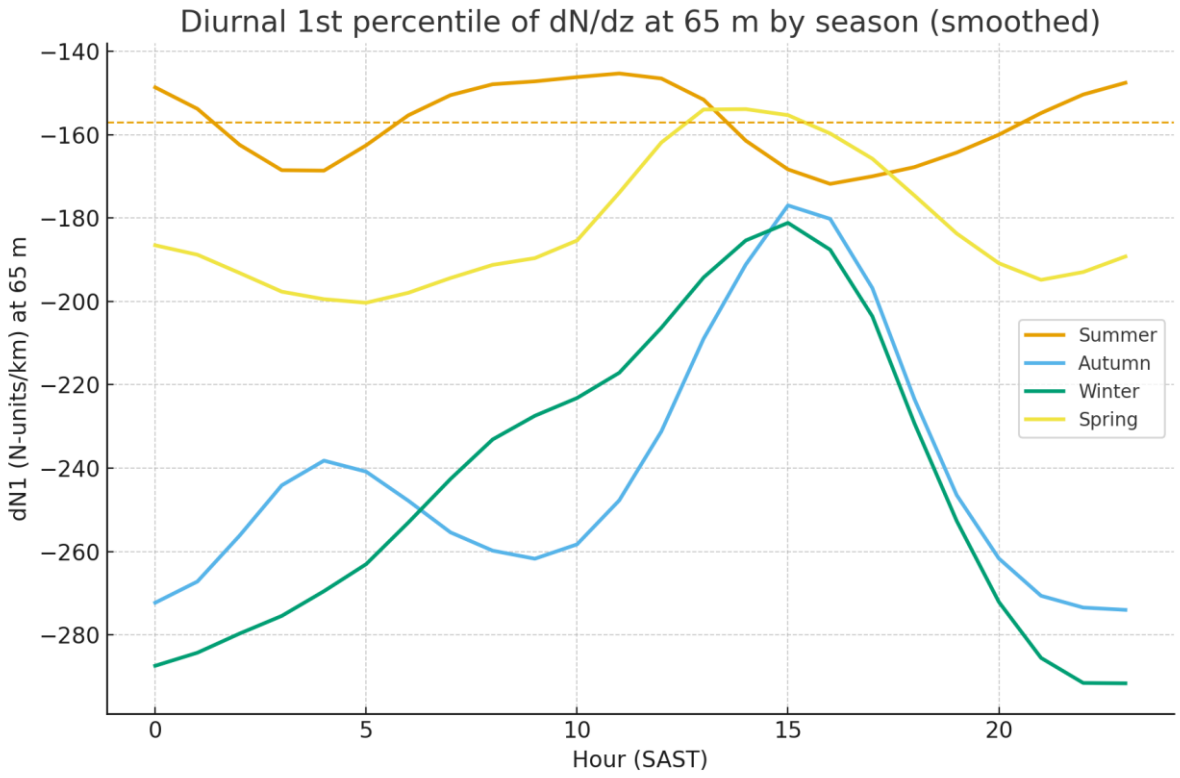


Figure 3. Line Plots of Diurnal Refractivity Gradient not exceeded for 1% of an average day

*Corresponding Author

The winter season possess the widest variability of about 111 N-unit/Km with a maximum and a minimum refractivity gradient of about -185 and -296 N-unit/Km occurring at 15:00 and 11:00 hours respectively. The diurnal variability of refractivity gradient during the autumn is in consonant with the winters but reduced to -95 N-unit/Km. The highest and lowest values of -178 N-unit/Km and -273 N-unit/Km were observed at similar times with winter. The low values of refractivity gradient observed at late night buttress the high probability of occurrence of the ducting in both seasons [30]. Although, ducting may be of great advantage, particularly in terrestrial radio broadcasts systems where reception is extended beyond coverage area, it poses a threat to radar systems as radio signal misses its intended target due to multiple ground reflections [32]. The spring possesses lower variability of about -44 N-unit/Km with a maximum and a minimum refractivity gradient of -156 N-unit/Km and -200 N-unit/Km observed at 13:00 and 5:00 hours respectively. The least variability was witnessed in the summer with occurrence of super refraction and ducting. Maximum and minimum gradients of -147 N-unit/Km and -175 N-unit/Km observed at 11:00 and 16:00 resulted to least variability of -28 N-unit/Km. Super refraction prevails from 6:00-13:00 and 21:00-2:00. Specifically, the ITU recommended standard refraction of -157 N-unit/Km were recorded at 2:00, 6:00, 13:00 and 21:00 hours. The seasonal diurnal differences align with radiometeorological theory, implying that nocturnal stability and near-surface humidity stratification steepen negative $dN/dz$ while daytime mixing increases $dN/dz$ toward less-negative values.

Conclusively, the summer is least affected while the winter is most affected by diurnal variation of atmospheric weather conditions. The reported refractivity gradients at 65 m capture the near-surface layer most relevant to terrestrial LOS links. It should be noted the figures 2 and 3 are built from hourly SAST data, hence they faithfully represent local timing of worst-case conditions which are crucial for local radio propagation data acquisition and for diagnosing recurrent pre-sunrise ducts versus afternoon benign periods [6] & [33].

**4.2 Monthly and Seasonal Statistics of Refractivity Gradient and Geoclimatic Factor**

The monthly CPDCs presented in Figure 4 shows a clear seasonal signature superimposed on month-to-month variability. Months in late autumn–winter (March-September) display heavier left tails, evidencing a higher frequency of strongly negative point gradients at 65 m. By contrast, late spring–summer (October-April) curves shift rightward, indicating fewer hours with large negative gradients. This pattern is physically consistent with a coastal boundary layer in which nocturnal stability, frequent shallow inversions and episodic frontal passages in winter steepen the vertical gradients of temperature and humidity, while daytime convective mixing and sea-breeze ventilation in summer relax them. The ERA5-driven, height-specific construction of refractivity (via ITU-R P.453-14) and the finite-difference estimate of $dN/dz$ at 65 m faithfully capture this near-surface control [6], [33]-[34] .

*Corresponding Author

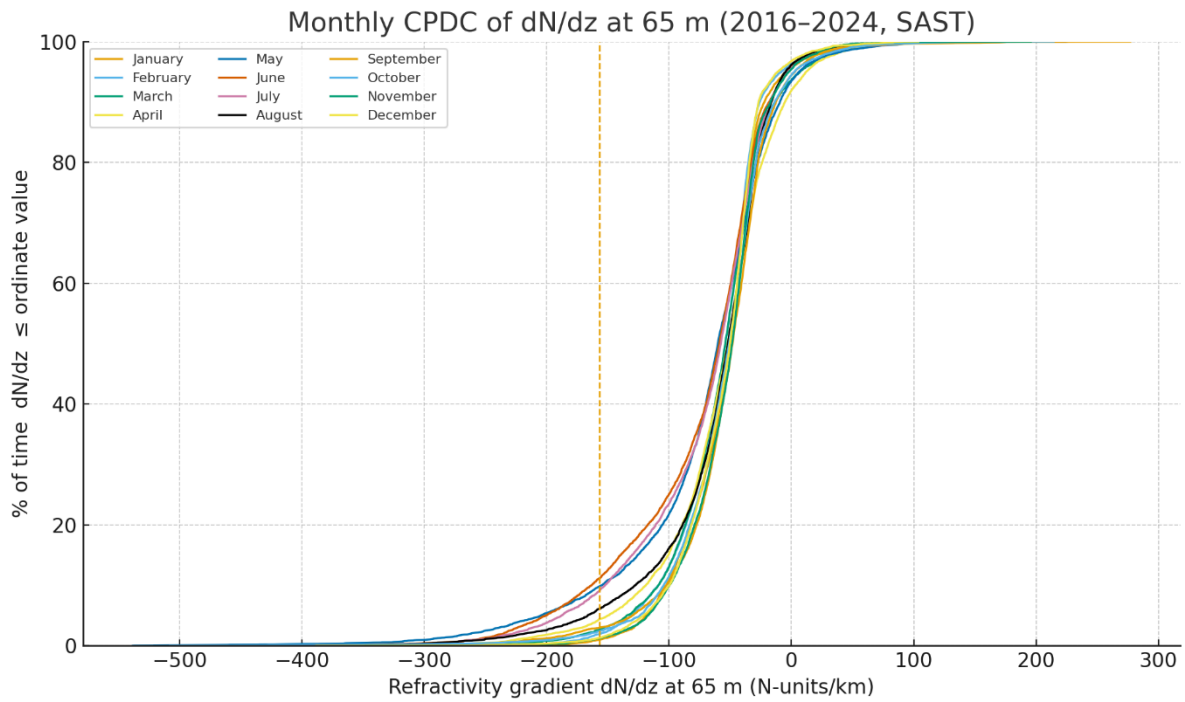


Figure 4. Cumulative Probability Distribution Curve of Monthly Refractivity Gradient

The monthly specific refractivity gradients at 1% non-exceedance in an average consolidates these distributions into a robust design statistic shown in Figure 5. The winter months consistently yield more negative than summer months, with transitional behaviour in autumn and spring. The intra-season dispersion, visible as non-monotonicity across adjacent months, likely reflects synoptic sequencing (front frequency, marine surges) and land–sea-breeze phasing, rather than noise, because there were no missing data during the computational analysis. For engineering interpretation, months with the most negative are those with highest trapping risk and hence greater fade-margin demands. Equation (6) shows that a more negative refractivity gradient implies a larger geoclimatic factor exponentially. As expected from Figures 5 and 6, Winter (JJA) exhibits the largest $K$and most negative $dN_1$, followed by Spring (SON); Summer (DJF) presents the lowest $K$ (least negative $dN_1$), with Autumn (MAM) intermediate. This ordering is typical of maritime south-coast climates, where cool-season stability and humidity stratification intensify super-refraction, while warm-season turbulent mixing mitigates it [30] & [35]. Because $K$ is an exponential transform of a tail statistic, a modest shift in $dN_1$can yield a noticeable change in $K$.

*Corresponding Author

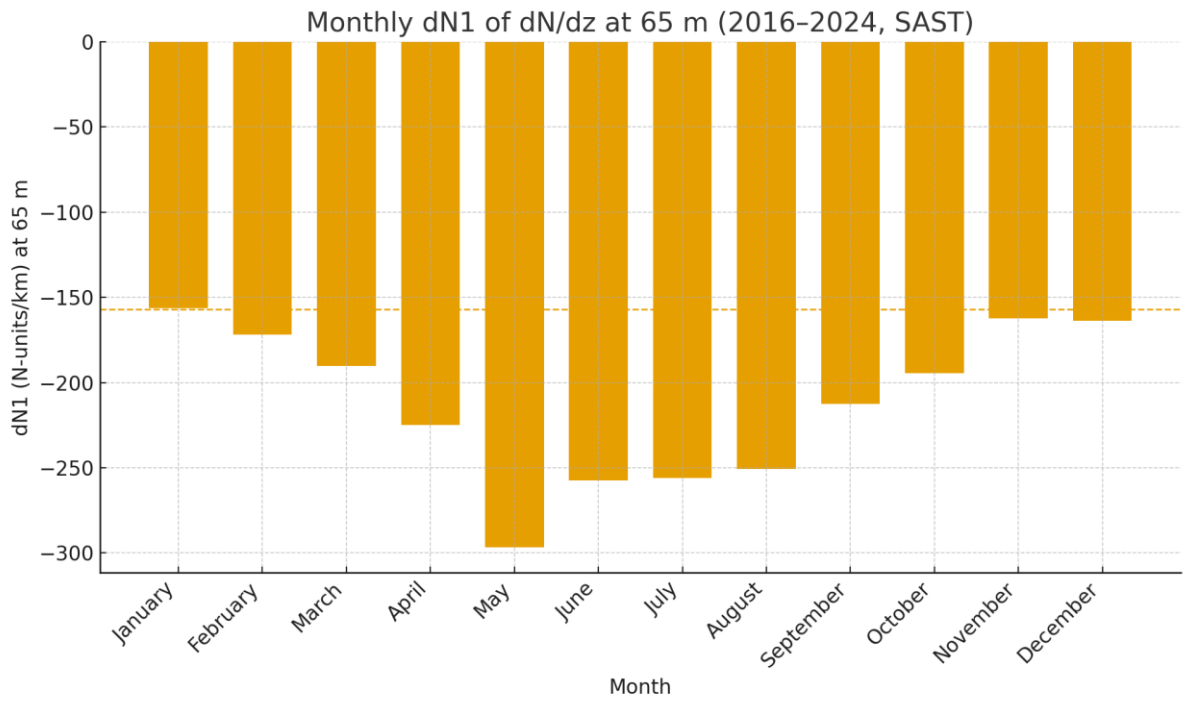


Figure 5. Bar chart of Monthly Refractivity Gradient not exceeded for 1% of an average year

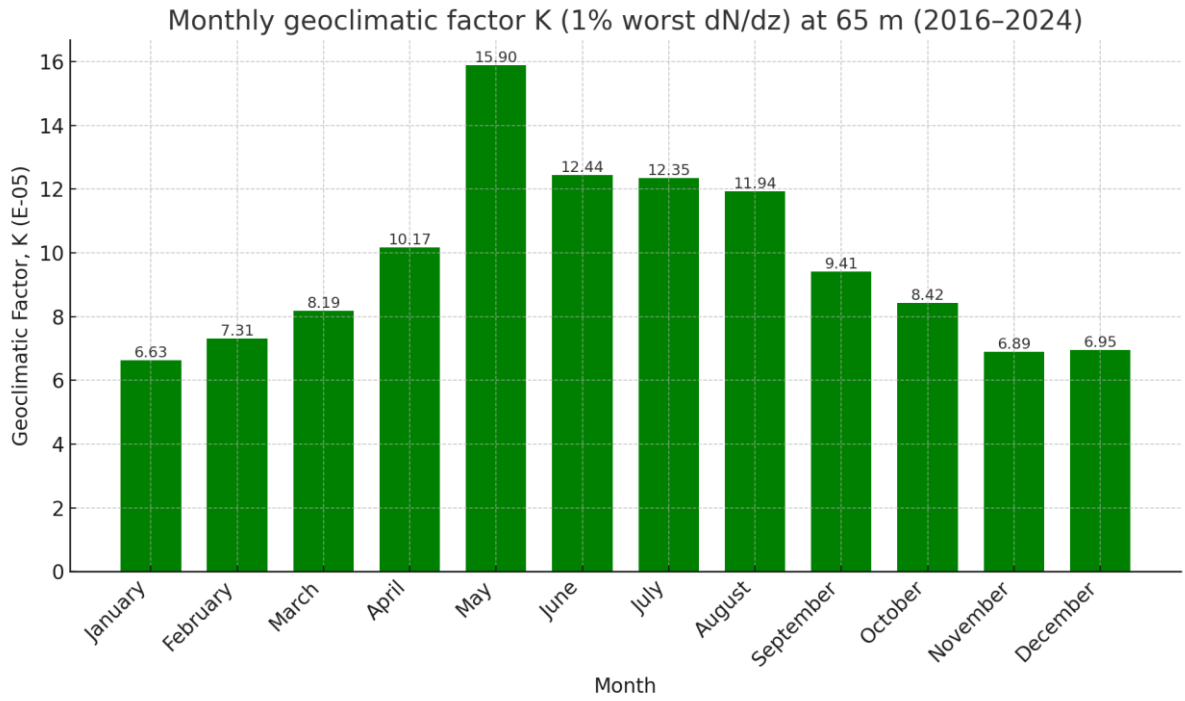


Figure 6. Bar chart of Monthly Geoclimatic Factor not exceeded for 1% of an average year

The statistics of the seasonal refractivity gradients and corresponding geoclimatic factors are presented in Table 1. The number of datapoints (*n_hours*) used for the mean computation, the upper and lower 95% CI of the mean *K*, and the percentage of ducting

*Corresponding Author

occurrence for each season are shown in the table. These metrics also confirmed the seasonal ordering established in the previous sub-section. Winter shows the largest of $12.29 \times 10^{-5}$ at 95% confidence interval (11.93–12.95) and highest ducting occurrence (8.8%), closely followed by Autumn with mean geoclimatic of $12.06 \times 10^{-5}$ and 5.6% ducting chances. Spring is intermediate ($8.25 \times 10^{-5}$; 2.2%), while Summer is lowest mean geoclimatic factor and ducting percentage of $7.01 \times 10^{-5}$; 1.4% respectively. Narrow CIs and large $n$-hours suggest stable estimates. Practically, fade-margin planning should adopt winter $K$ for worst-case design and summer $K$ for optimistic baselines, consistent with boundary-layer theory linking stronger nocturnal stability to more negative $dN/dz$.

Table 1. Statistics of the seasonal Refractivity Gradients and Geoclimatic Factor

| Season | n_hours | Mean K (E-05) | K_CI95_low (E-05) | K_CI95_high (E-05) | Ducting fraction (%) |
|---|---|---|---|---|---|
| Summer | 19510 | 7.01 | 6.9 | 7.13 | 1.4 |
| Autumn | 19872 | 12.06 | 11.49 | 12.71 | 5.6 |
| Winter | 19872 | 12.29 | 11.93 | 12.95 | 8.8 |
| Spring | 19656 | 8.25 | 7.87 | 8.49 | 2.2 |

The consistency across Figures 4–6 and Table 1, from distributional shape to monthly extremes and seasonal aggregates, adds confidence that the ERA5-based, height-aware methodology is capturing physically coherent refractivity dynamics at 65 m in Port Elizabeth, suitable for site-specific design envelopes and fade-margin budgeting.

**4.3 Annual trend of Geoclimatic Factor**

The annual trend of K over the studied period was investigated by computation and analysis of the yearly average values. Figure 7 depicts a modest interannual spread in the annual geoclimatic factor, with values clustering between $9.0 \times 10^{-5}$and $10.5 \times 10^{-5}$. A local maximum of $10.38 \times 10^{-5}$ in 2019 and a minimum of $8.69 \times 10^{-5}$ in 2021 bracket a recovery through 2022–2024 after a dip in 2021. These fluctuations primarily reflect changes in the 1% most-negative point refractivity gradient at 65 m mostly influenced by the frequency and intensity of near-surface inversions and humidity stratification.

*Corresponding Author

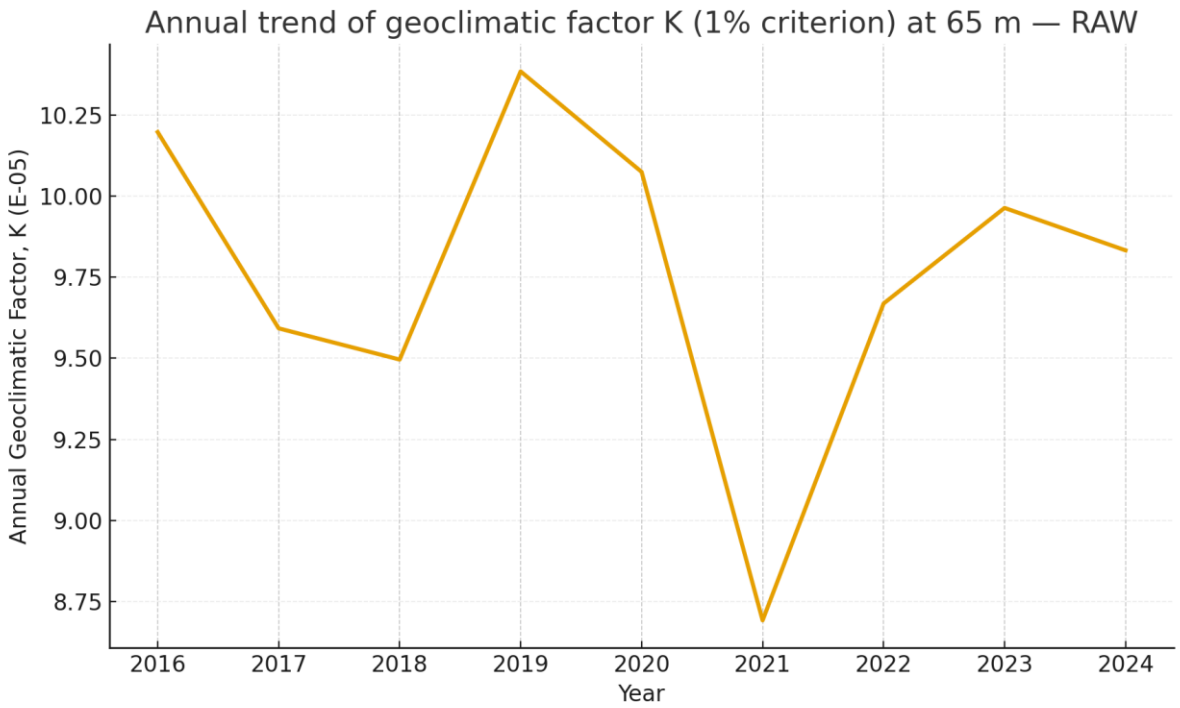


Figure 7. Annual trend of Geoclimatic Factor not exceeded for 1% of an average year

The 2019 peak implies more stronger negative refractivity gradient, consistent with episodes of persistent nocturnal stability and moisture stratification in the marine boundary layer, conditions that favour trapping and ducting. Conversely, the all-year low value of $8.69 \times 10^{-5}$ observed 2021 indicates a year with weakest negative refractivity gradients occasioned by fewer and shallower inversions, and stronger daytime or synoptic-scale mixing. Physically, such a reduction arises when cool, well-mixed boundary layers and frequent frontal or onshore wind passages erode the vertical contrast of temperature and humidity across the lowest 0–150 m altitude, shifting $dN/dz$ toward less-negative values and lowering $K$. The 2021 dip is consistent with large-scale climate forcing plus local boundary-layer physics reported by some previous research on South Africa climate. The South African annual state of climate officially documents La Niña state and spatially heterogeneous rainfall anomalies during the 2020/21 hydrological year. This phase shifts storm tracks and moisture transport, with widespread above-normal summer rainfall inland and notable regional contrasts toward the southern coastal zones such as Port Elizabeth. Such regime alter near-surface lapse rates (temperature inversion and humidity stratification) and mixing in the marine boundary layer [36]-[37]. Summarily, the La Niña-driven circulation, rainfall anomalies and the radio-meteorological dependence of $K$ on boundary-layer stability provide a coherent explanation for the observed dip in 2021. This behaviour is well established in refractivity theory and marine-ducting studies, which show $K$ and duct occurrence to be highly sensitive to boundary-layer stability, moisture stratification, above-normal rainfall and synoptic variability [38]-[40]. The subsequent years depict a sharp recovery of K attributed to relaxation of La Niña state and normalized rainfall followed by a drop in 2024. The overall annual K throughout the study period is $9.86 \times 10^{-5}$ which correspond to annual refractivity gradient of

**4.4 Practical recommendations for inter-terrestrial link design**

*Corresponding Author

The findings of the study hereby recommend the annual $K$ derived for Port Elizabeth and its environs as the baseline design value in link budgets and availability studies. For mission-critical or season-sensitive links, substitute the seasonal $K$ presented in Table 1, especially the winter value, to size a higher fade margin and constrain paths more conservatively, since larger $K$ reflects a more negative $dN_1$ and stronger ducting propensity [5], [34] & [41]. Schedule maintenance and high-throughput operations away from the pre-dawn window, when the diurnal 1% envelope indicates the deepest negative gradients. Such operations should be executed in the afternoon periods when mixing weakens refractivity gradients. Combine this K selection technique with adaptive modulation and coding and power control to ride through transient super-refraction episodes.
Keep antenna height fixed at 65 m or re-compute $K$ if site height, terrain or nearby land-use changes, because small vertical shifts in the first 150 m can materially alter $dN/dz$. When planning new routes, prioritize shorter spans, higher clearances, and diversity (path or frequency) for links exposed to wintertime marine inversions. Finally, review $K$annually as longer records accrue and re-validate against ERA5-based CPDCs and 1% statistics. These recommendations align with ITU-R guidance to use representative, site-specific climatology for Line-of-sight (LOS) design [5]-[6], [33]-[34].

## 5.0 CONCLUSION

This study quantified the near-surface refractivity gradient and geoclimatic factor for inter-terrestrial links at 65 m AGL in Port Elizabeth using hourly ERA5 meteorological data mapped to height and evaluated with the ITU-R P.453-14 refractivity and $K$ formulation. Diurnally, the 1% envelopes showed pre-dawn minima refractivity gradient, relaxing through the afternoon. Seasonally, winter exhibited the most negative gradient and largest $K$, autumn and spring, while summer possesses the least. Interannually, $K$ varied modestly throughout the study period (2016-2024), with a temporary minimum in 2021, consistent with enhanced boundary-layer mixing and reduced inversion frequency, which attenuate moisture, temperature stratification and lessen super-refraction. These patterns are physically coherent and statistically stable, supporting use of the annual $K$ for baseline design and seasonal $K$, especially winter value, for mission-critical margining. The derived radio propagation parameters are recommended for inter-terrestrial link design in Port Elizabeth and its environs. The methodological approach used for this study is reproducible and site-specific and can be extended to other South African locations and heights to refine regional design envelopes and availability targets.

## ACKNOWLEDGEMENT

The authors wish to appreciate the Tshwane University of Technology for the supports provided during the course of this project.

## REFERENCES

[1] M. M. Tanko, M. S. Liman, W. L. Lumbi, U. S. Aliyu, and M. U. Sarki, “Field strength variability mapping of Nigeria”, *Journal of the Nigerian Society of Physical Sciences*, vol. 4, (2022), p. 746. https://doi.org/10.46481/jnsps.2022.746

*Corresponding Author

[2] Y. B. Lawal and E. T. Omotoso, "Investigation of point refractivity gradient and geoclimatic factor at 70 m altitude in Yenagoa, Nigeria", *Journal of the Nigerian Society of Physical Sciences*, vol. 5, (2023), p. 1081. https://doi.org/10.46481/jnsps.2023.1081

[3] Y. B. Lawal and A. G. Ashidi, "Statistical estimation of effective Earth radius factor over Lagos using radiosonde data", *International Journal of Multidisciplinary and Current Research*, vol. 5, (2017), p. 343.

[4] K. O. Suleman et al., "Investigation of diurnal and seasonal variation of radio refractivity, refractivity gradient, k-factor, and field strength over Ogbomoso, Nigeria", *International Journal of Recent Technology and Engineering*, vol. 29, (2025), pp. 1–8.

[5] ITU-R, *Recommendation ITU-R P.453-14: The radio refractive index: Its formula and refractivity data*, (2019).

[6] ITU-R, *Recommendation ITU-R P.530-19: Propagation data and prediction methods required for the design of terrestrial line-of-sight systems*, (2025).

[7] A. O. Akanni and J. M. Adekunle, "Influence of geoclimatic factor on fade depth for wireless link design using radiosonde data", *International Journal of Research and Innovation in Applied Science*, vol. 5, (2020), pp. 145–150.

[8] A. M. Nyete and T. J. O. Afullo, "On the k-factor distribution and diffraction fading for Southern Africa", *African Research Journal*, vol. 101, no. 4, (2010), pp. 3–10.

[9] A. T. Adediji, M. O. Ajewole, and S. E. Falodun, "Distribution of radio refractivity gradient and effective Earth radius factor (k-factor) over Akure, South-Western Nigeria", *Journal of Atmospheric and Solar-Terrestrial Physics*, vol. 73, no. 16, (2011), pp. 2300–2304. https://doi.org/10.1016/j.jastp.2011.06.017

[10] A. M. Nyete and T. J. O. Afullo, "Seasonal distribution modeling and mapping of the effective Earth radius factor for microwave link design in South Africa", *Progress in Electromagnetics Research B*, vol. 51, (2013), pp. 1–32. https://doi.org/10.2528/PIERB13030406

[11] P. K. Odedina and T. J. O. Afullo, "Use of spatial interpolation technique for determination of geoclimatic factor and fade depth calculation in Southern Africa", *IEEE Africon*, vol. 51, (2007), pp. 1–5.

[12] Y. Bettouche, T. Youssef, and M. Hadi, "Geoclimatic factor and point refractivity evaluation in Quebec-Canada", *URSI GASS Proceedings*, (2014).

[13] I. J. Etokebe, M. C. Uko, and I. U. Chinwe, "Determination of refractivity gradient and geoclimatic factor using radiosonde data and inverse distance weighting spatial interpolation", *International Journal of Systems Science and Applied Mathematics*, vol. 1, no. 4, (2016), pp. 76–81.

[14] M. Tarek, F. P. Brissette, and R. Arsenault, "Evaluation of the ERA5 reanalysis as a potential reference dataset for hydrological modelling", *Hydrology and Earth System Sciences*, vol. 24, (2020), pp. 2527–2544. https://doi.org/10.5194/hess-24-2527-2020

[15] O. J. Abimbola, B. Adeyemi, I. Emmanuel, and A. Atoyebi, "Estimation of radio refractivity from satellite-derived meteorological data for West Africa", *Atmospheric Research*, vol. 250, (2021), p. 105368. **Correct DOI:** https://doi.org/10.1016/j.atmosres.2020.105368

[16] Y. B. Lawal, P. A. Owolawi, C. Tu, E. Van Wyk, and J. S. Ojo, "Analysis of cross-polarization discrimination due to rain height over selected satellite links in South Africa", *Atmosphere*, vol. 16, no. 3, (2025), p. 256. https://doi.org/10.3390/atmos16030256

[17] I. Emmanuel, B. Adeyemi, and K. D. Adedayo, "Estimation of refractivity gradient and geoclimatic factor for radio link design in Nigeria", *Physical Science International Journal*, vol. 19, (2018), pp. 1–15. https://doi.org/10.9734/PSIJ/2018/43571

[18] D. M. Pastore et al., "Comparison of atmospheric refractivity estimation methods using CASPER-East observations", *Radio Science*, vol. 56, no. 5, (2021), e2020RS007244. https://doi.org/10.1029/2020RS007244

[19] I. B. Oluwafemi and M. O. Olla, "Estimation of geoclimatic factor for Nigeria through meteorological data", *European Journal of Electrical Engineering and Computer Science*, vol. 5, no. 3, (2021), pp. 43–49.

[20] A. J. Palmer and D. C. Baker, "Predicting the long-term average of the effective Earth radius factor for South Africa using ground-based observations", *SAIEE Africa Research Journal*, vol. 97, no. 2, (2021), pp. 182–185. https://doi.org/10.23919/SAIEE.2021.9443731

[21] A. J. Palmer and D. C. Baker, "Predicting the monthly cumulative distribution of the effective Earth radius factor for South Africa", *IEEE Africon*, (2004), pp. 1007–1010. https://doi.org/10.1109/AFRICON.2004.1406787

*Corresponding Author

[22] Y. B. Lawal, S. E. Falodun, and J. S. Ojo, "Temporal evolution of atmospheric parameter-profiling on rain height over two geoclimatic regions in Nigeria", *Journal of Atmospheric and Solar-Terrestrial Physics*, vol. 211, (2020), p. 105482. https://doi.org/10.1016/j.jastp.2020.105482

[23] A. C. Kruger, and M. P. Nxumalo. "Historical Rainfall Trends in South Africa: 1921-2015" *Water SA* , vol. 43, (2017), pp. 285–297. https://doi.org/10.4314/wsa.v43i2.12

[24] A. L. Sheu, J. S. Ojo, and A. M. Aibinu, "Investigation of the vertical profile radio refractivity gradient and effective Earth-radius factor (k-factor) in transmission link over Oyo, Nigeria", *Tanzania Journal of Science*, vol. 48, no. 1, (2022), pp. 1–13.

[25] D. O. Akpootu, M. Idris, I. Nouhou, M. I. Iliyasu, and A. O. Aina, "Estimation and investigation of variability of tropospheric radio refractivity and radio field strength over Accra, Ghana", *Journal of Atmospheric and Earth Science*, vol. 5, (2021), p. 026.

[26] A. A. Willoughby, M. M. Tanko, H. D. Musa, and M. S. Abdullahi, "Estimation of some radio propagation parameters using radiosonde measurements over Nigeria", *Journal of the Nigerian Society of Physical Sciences*, vol. 5, (2023), p. 875. https://doi.org/10.46481/jnsps.2023.0875

[27] S. D. Gunashékar, "Transhorizon radiowave propagation due to evaporation ducts", *Resonance*, vol. 11, no. 1, (2006), pp. 51–62. https://doi.org/10.1007/BF02834828

[28] C. Tepecik and H. Erol, "Atmospheric refractivity estimation from radar sea clutter using refractivity from clutter technique", *Radio Science*, vol. 55, no. 5, (2020), e2019RS006911. https://doi.org/10.1029/2019RS006911

[29] Copernicus Climate Change Service (C3S), "ERA5 hourly data on pressure levels from 1940 to present", (2023). https://cds.climate.copernicus.eu/datasets/reanalysis-era5-pressure-levels?tab=download)

[30] P. D. Tyson, R. A. Preston-Whyte, and R. Diab, "Towards an inversion climatology of Southern Africa: Part I, surface inversions", *South African Geographical Journal*, vol. 58, no. 2, (1976), pp. 151–163. https://doi.org/10.1080/03736245.1976.10559577

[31] N. R. K. Murthy, S. Vijaya, and B. Rao, "Studies on the occurrence of duct and superrefraction over Indian region", *International Journal of Current Research and Review*, vol. 5, no. 12, (2013), pp. 12–20.

[32] G. Guanjun and L. Shukai, "Study on the vertical profile of refractive index in the troposphere", *International Journal of Infrared and Millimeter Waves*, vol. 21, no. 7, (2000), pp. 1103–1112. https://doi.org/10.1023/A:1006402227010

[33] H. Hersbach et al., "The ERA5 global reanalysis", *Quarterly Journal of the Royal Meteorological Society*, vol. 146, no. 730, (2020), pp. 1999–2049. https://doi.org/10.1002/qj.3803

[34] E. K. Smith and S. Weintraub, "The constants in the equation for atmospheric refractive index at radio frequencies", *Proceedings of the IRE*, vol. 41, no. 8, (1953), pp. 1035–1037. https://doi.org/10.1109/JRPROC.1953.274297

[35] Y. B. Lawal, P. A. Owolawi, C. Tu, E. Van Wyk, and J. S. Ojo, "The kernel density estimation technique for spatio-temporal distribution and mapping of rain heights over South Africa", *Atmosphere*, vol. 15, no. 7, (2024), p. 1354. https://doi.org/10.3390/atmos15071354

[36] SAWS, *Annual State of the Climate of South Africa 2021*, (2022).

[37] DWS, *National State of Water Report 2021*, (2022).

[38] S. Mentes and Z. Kaymaz, "Investigation of surface duct conditions over Istanbul, Turkey", *Journal of Applied Meteorology and Climatology*, vol. 46, no. 3, (2007), pp. 318–337. https://doi.org/10.1175/JAM2452.1

[39] Q. Jiang, Q. Wang, and S. Gaberšek, "Mesoscale variability of surface ducts during Santa Ana wind episodes", *Journal of Geophysical Research: Atmospheres*, vol. 127, no. 9, (2022), e2022JD036698. https://doi.org/10.1029/2022JD036698

[40] Y. Zhou, Y. Liu, J. Qiao, J. Li, and C. Zhou, "Statistical analysis of the spatiotemporal distribution of lower atmospheric ducts over the seas adjacent to China", *Remote Sensing*, vol. 14, no. 19, (2022), p. 4864. https://doi.org/10.3390/rs14194864

[41] ITU-R, *Recommendation ITU-R P.834-9: Effects of tropospheric refraction on radiowave propagation*, (2017).

*Corresponding Author

*Corresponding Author